Front. Mater. Sci. 2019, 13(2): 145–155
https://doi.org/10.1007/s11706-019-0455-2

RESEARCH ARTICLE

Preparation of sulfur-doped graphene fibers and their application in flexible fibriform micro-supercapacitors

Bin CAI[1], Changxiang SHAO[2], Liangti QU[2], Yuning MENG (✉)[1], and Lin JIN (✉)[3]

1 School of Chemistry and Chemical Engineering, Zhoukou Normal University, Zhoukou 466001, China
2 Key Laboratory of Photoelectronic/Electrophotonic Conversion Materials, Key Laboratory of Cluster Science (Ministry of Education), School of Chemistry and Chemical Engineering, Beijing Institute of Technology, Beijing 100081, China
3 The Key Laboratory of Rare Earth Functional Materials and Applications, Zhoukou Normal University, Zhoukou 466001, China

ABSTRACT: A novel type of sulfur-doped graphene fibers (S-GFs) were prepared by the hydrothermal strategy, the *in situ* interfacial polymerization method and the annealing method. Two S-GFs were assembled into an all-solid-state fibriform micro-supercapacitor (micro-SC) that is flexible and has a high specific capacitance (4.55 mF·cm^{-2}) with the current density of 25.47 μA·cm^{-2}. The cyclic voltammetry (CV) curve of this micro-SC kept the rectangular shape well even when the scan rate reached 2 V·s^{-1}. There is a great potential for this type of S-GFs used in flexible wearable electronics.

KEYWORDS: graphene fiber; sulfur doping; wearable electronics; flexible supercapacitor; micro-supercapacitor

Contents

Received December 24, 2018; accepted January 29, 2019

E-mails: ynmeng88@126.com (Y.M.), jinlin_1982@126.com (L.J.)

1 Introduction

Flexible and wearable electronic devices that represent a mainstream direction in modern electronics have continuously attracted attention owing to their realizable small diameters, light weight, and suitability for integration into textiles [1–9]. People have been pursuing various highly flexible, light weight, portable and wearable energy storage devices, one kind of which are micro-supercapacitors (micro-SCs) that have been focused on by scientific researchers. Graphene fibers (GFs), a kind of macroscopic and one dimensional (1D) materials, assembled by

graphene sheets, have been widely used in flexible wearable electronic devices due to their virtues such as light weight, flexibility for textiles and ease of modification and functionalization [10–18]. Although micro-SCs, with derived advantages from both GFs and supercapacitors, have been studied widely [18–29], there is still a major challenge towards viable applications for this kind of devices. Compared with traditional planar supercapacitors, micro-SCs have much lower energy density and power density, which is a serious problem difficult to solve. Therefore, more attention has been focused on increasing values of the capacitance and the energy density of micro-SCs. In our previously reported work, such two values mentioned above reached up to 9.1–9.6 $mF \cdot cm^{-2}$ and 1.7×10^{-7} $W \cdot h \cdot cm^{-2}$, respectively [18,24]. Notably, these results still need to be further improved.

To tailor electrochemical properties of graphene-based conductive materials, the chemical doping is considered as an effective method. Recently, nitrogen, boron, sulfur and phosphorus have been selected as doped heteroatoms to enhance the capacitive performance of graphene-based materials [30–38]. Compared with undoped ones, sulfur-doped graphene-based materials demonstrated enhanced electrochemical properties [37–41], while nitrogen-doped porous GFs showed significant improvement in the electrochemical performance [35]. However, to the best of our knowledge, the performance of sulfur-doped graphene fibers (S-GFs) used as supercapacitor electrodes has not been reported yet.

As an important polythiophene derivative, poly(3,4-ethylenedioxythiophene) (PEDOT) is often used as an active material in capacitor electrodes due to its excellent properties such as high conductivity and thermal stability, fast chargeable/dischargeable features, and high electrochemical stability [42–45]. Till now, the reports on using sulfur deriving from PEDOT as the doped element in carbon nanostructures are still rare [38].

Herein, we report our research in S-GFs used as electrode materials in flexible fibriform micro-SCs. First, we fabricated GFs by the dimensionally-confined hydrothermal strategy; second, we used the *in situ* interfacial polymerization method to coat PEDOT on GFs; third, PEDOT-GFs were annealed in an argon atmosphere. By the third process, the sulfur element deriving from PEDOT can be incorporated successfully into GFs and contribute to the high capacitance [38]. We assembled two S-GFs into a fibriform micro-SC by intertwining them with the poly (vinyl alcohol)–sulphuric acid (PVA–H_2SO_4) gel electrolyte. Compared with pure GF micro-SCs, the assembled micro-SC displays many advantages including more flexibility, larger specific capacitance, and higher cycling stability and energy density. It is believed that this type of S-GFs will contribute to the development of flexible wearable electronics.

2 Experimental

2.1 Chemicals

All chemicals including graphene oxide (GO) powder, 3,4-ethylenedioxythiophene (EDOT) (98%), $LiClO_4$ (98%), $FeCl_3$ (98%), absolute ethanol, PVA (n = (1750±50)) and H_2SO_4 (98%) were from commercial sources and used without further purification. All aqueous solutions were got by tri-distilled water.

2.2 Process of the S-GF preparation and the sulfur-doped micro-SC fabrication

2.2.1 Preparation of GFs

GFs were got by the dimensionally-confined hydrothermal strategy described in our previous paper with a slight modification [18]. Briefly, 8 $mg \cdot mL^{-1}$ of the GO solution was firstly injected into the glass pipelines (inner diameter: 0.4 mm) with two ends sealed up. Subsequently, the glass pipelines were put into an oven, heated to 230 °C, maintained at this temperature for 2 h, and naturally cooled to room temperature. Lastly GFs were released manually.

2.2.2 Preparation of PEDOT-GFs

PEDOT-GFs were prepared by the *in situ* interfacial polymerization method mentioned in our previous work [44]. Briefly, at first the EDOT–$FeCl_3$–ethanol solution (the concentrations of both $FeCl_3$ and EDOT are 0.05 $g \cdot mL^{-1}$) (Solution A) was prepared. Then, the synthesized GFs were immersed into Solution A for 1 min. With the evaporation of ethanol, EDOT started to polymerize on the surface of GFs, leading to the formation of the PEDOT shell. After 1 h, PEDOT-GFs were obtained. The fibers were washed for three times by deionized water and lastly dried in air.

2.2.3 Preparation of S-GFs

In an argon atmosphere, the air-dried PEDOT-GFs placed

in a tube were annealed at 800 °C for 3 h. The heating rate was 5 °C/min. In this process, the sulfur element deriving from PEDOT was successfully doped into GFs, resulting in the formation of S-GFs.

2.2.4 Fabrication of the fibriform sulfur-doped micro-SC

Preparation of the PVA–H_2SO_4 gel electrolyte: Firstly, under vigorous stirring, 1 g PVA powder and 10 mL water were added into a 50 mL beaker which was heated to 85 °C. Then 1 g H_2SO_4 (98%) was added into the clear solution under stirring for 30 min. Finally, the gel electrolyte was kept at 85 °C without stirring. Preparation of fibriform sulfur-doped micro-SC: Two S-GFs were precoated with the PVA–H_2SO_4 gel electrolyte, dried in air, and then intertwined manually to form the all-solid-state fibriform sulfur-doped micro-SC.

2.3 Instruments

The morphologies of GFs, S-GFs and the fibriform micro-SC were revealed by scanning electron microscopy (SEM, Hitachi S-3000N). The acceleration voltage was 10 kV. We used a Kratos Axis Ultra DLD equipped with a monochromatic Al-Kα X-ray source to get X-ray photoelectron spectroscopy (XPS) spectra. The energy dispersive spectroscopy (EDS) mapping was taken on JSM-7001F SEM unit. Raman spectra were recorded on a LabRAM HR Evolution, HORIBA Jobin Yvon, France. The wavelength is 532 nm with an Ar laser. Electrochemical properties were tested with a CHI660E electrochemical workstation.

2.4 Electrochemical characterization

First, GFs and S-GFs were investigated as working electrodes in a three-electrode system (electrolyte: 1 mol·L^{-1} $LiClO_4$ solution; counter electrode: Pt wire; reference electrode: Ag/AgCl (3 mol·L^{-1} KCl)). Second, we tested electrochemical properties of the fibriform micro-SC in a two-electrode system by using cyclic voltammetry (CV) and galvanostatic charge–discharge (GCD) measurements. The flexibility and the electrochemical stability of the micro-SC at the bending state were also studied.

3 Results and discussion

3.1 Preparation of S-GFs and SEM, EDS mapping and XPS results

Figure 1 shows the preparation of S-GFs schematically. PEDOT-GFs were firstly prepared by the hydrothermal strategy and the *in situ* interfacial polymerization method. Then, PEDOT-GFs were annealed in an argon atmosphere, and lastly S-GFs were obtained.

The initial GFs and the obtained S-GFs were analyzed by SEM, and the results are shown in Fig. 2. Obviously, GFs have a rough and wrinkled surface. The diameter of the initial GF is 30 μm (Figs. 2(d)–2(f)), which increased to 90 μm after coating with PEDOT [44]. After annealing, the sulfur from PEDOT was incorporated successfully into the wrinkled graphene sheets, contributing to the electron transportation. The diameter of the S-GF is about 25 μm and its surface morphology is shown in Figs. 2(a)–2(c). The mechanical stability of S-GFs is comparable to that of pure GFs (Fig. S1).

The EDS mapping data indicate that the sulfur element is distributed uniformly over the outside of a GF (Figs. 3(a) and S2). The weight and atomic percents of the sulfur element are 2.02% and 0.82%, respectively, within the confined area outlined in Fig. S2(a). The XPS full profiles of GFs and S-GFs reveal that the sulfur atoms were successfully doped into GFs (Fig. 3(b)). Unlike undoped GFs, there are two visible peaks at 164.9 and 228.8 eV, corresponding to S 2p and S 2s (Fig. 3(b)), respectively.

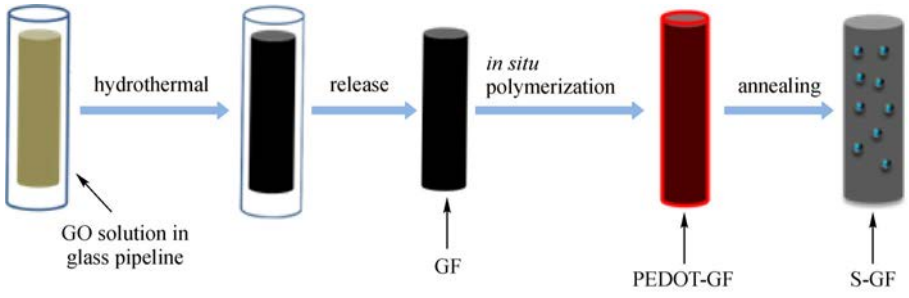

Fig. 1 Schematic of the preparation of S-GFs.

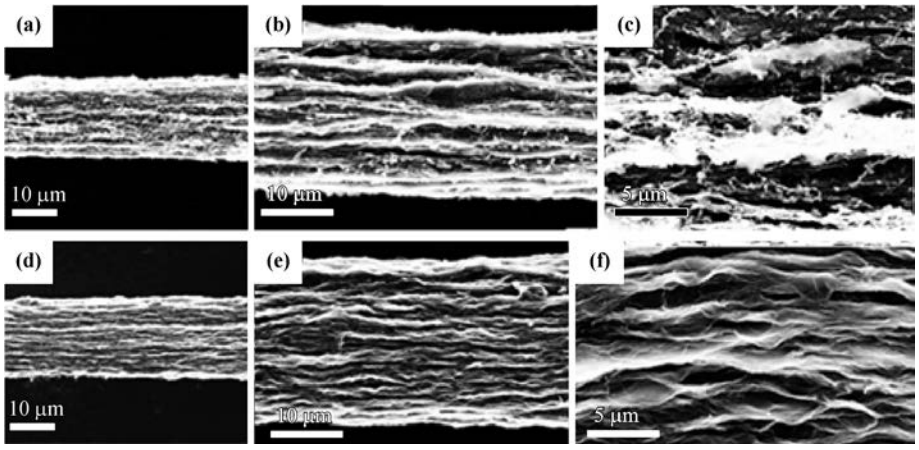

Fig. 2 SEM images of **(a)(b)(c)** an S-GF and **(d)(e)(f)** a pure GF at different scales.

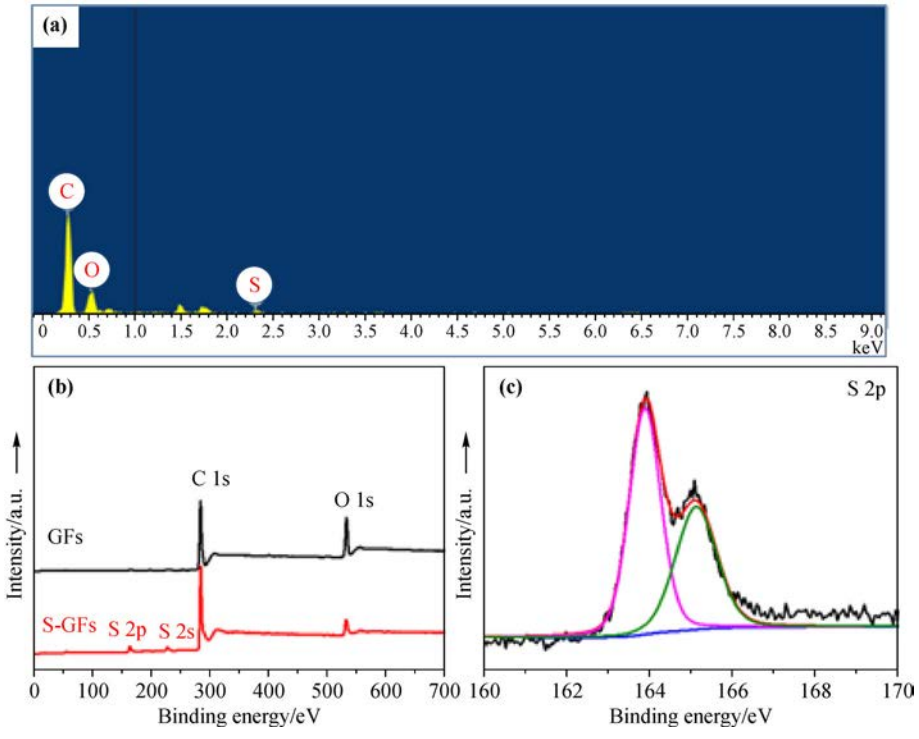

Fig. 3 **(a)** The EDS result of S-GFs. **(b)** XPS survey spectra of GFs and S-GFs. **(c)** The S 2p spectrum of S-GFs.

The higher solution S 2p profile (Fig. 3(c)) of S-GFs presents a pair of peaks at 163.9 and 165.0 eV, indicating that the sulfur atoms have been doped into GFs with the structure of C–S–C [38]. The C 1s spectrum can be deconvoluted into three fitted subpeaks (Fig. S3). The peak located at 284.8 eV is appointed to the graphitic bonding of sp^2 C=C, while the peak at 286.1 eV to sp^3 C and C=C, and the peak at 288.1 eV to O–C=O [35]. The proof for the sulfur doping in GFs was also provided by Raman spectra (Fig. S4). Compared with the G peak of GFs at 1599 cm^{-1}, the G peak of S-GFs is shifted to 1590 cm^{-1}, which is a critical feature of the n-type doped graphene [40,46]. It is observed that a similar red shift for the nitrogen-doped graphene was reported previously [47–48]. In general, the intensity ratio of the G band to the D band (I_G/I_D) can tell us the information of the structural change. A low I_G/I_D ratio suggests the high extent of disorder [38,49–50]. The I_G/I_D values were determined to be 0.93 and 0.87 for GF and S-GF, respectively. The lower I_G/I_D of S-GFs indicates that there are more defects in GFs due to the sulfur doping. Such Raman spectra combined with results from EDS mapping and XPS confirm that the sulfur

element has been doped into GFs successfully, and the fabrication method is feasible at the same time.

3.2 Electrochemical performance of the all-solid-state fibriform micro-SC

CV was used to evaluate the electrochemical performance of S-GFs. In Fig. 4(a), the CV curves of S-GFs show ideal capacitive behaviors when the scan rate ranges from 10 to 800 $mV \cdot s^{-1}$, comparable to our previous work and is attributed to the doped sulfur element. The sulfur element accelerates the ion transportation, and at the same time, the core GF has high capacitive behavior [44]. Actually, the nearly rectangular shape could be kept even the scan rate reached up to 2.8 $V \cdot s^{-1}$ (Fig. S5). The initial GFs present a shuttle shape of CV curves corresponding to different scan rates, especially when the scan rate is up to 300 $mV \cdot s^{-1}$ (Fig. 4(b)), which is caused by the dense structure of GFs [44]. Furthermore, compared with that of pure GFs, the CV curve of S-GFs (Fig. 4(c)) clearly shows that S-GFs have a better energy-storage ability and higher rate performance [44] when the scan rate is 800 $mV \cdot s^{-1}$.

As S-GFs have high flexibility and electrochemical capacitive behavior, we fabricate a symmetric all-solid-state fibriform supercapacitor by intertwining two S-GFs with the PVA–H_2SO_4 gel electrolyte. In this fiber supercapacitor, two S-GFs act as two electrodes. The assembled fiber supercapacitor possesses flexibility and mechanical stability inherited from the electrodes (Figs. 5(a) and 5(b)). Figure 5(c) shows that the two fibers are connected by the PVA–H_2SO_4 gel electrolyte. However, the cross-section view (Fig. 5(d)) reveals that the two fibers are not contacted with each other directly avoiding the short circuit. Compared with the liquid electrolyte, the PVA–H_2SO_4 gel electrolyte overcomes many drawbacks, such as leakage of electrolyte, difficulty in device encapsulation, and environmental unfriendliness. Besides acting as the electrolyte, the layer of PVA–H_2SO_4 along S-GFs can keep the two electrodes apart to avert the undesirable short circuit.

CV and GCD measurements of the fiber capacitor have been performed in a two-electrode system to characterize electrochemical properties. Figure 6(a) reveals CV curves of the fibriform supercapacitor assembled by two S-GF electrodes and the PVA–H_2SO_4 gel electrolyte with increasing the scan rate from 0.01 to 1 $V \cdot s^{-1}$ in an electrochemical window from −0.4 to 0.6 V. The CV curves show similar shape of a quasi-rectangular, confirming that throughout the electrode, there are efficient electric

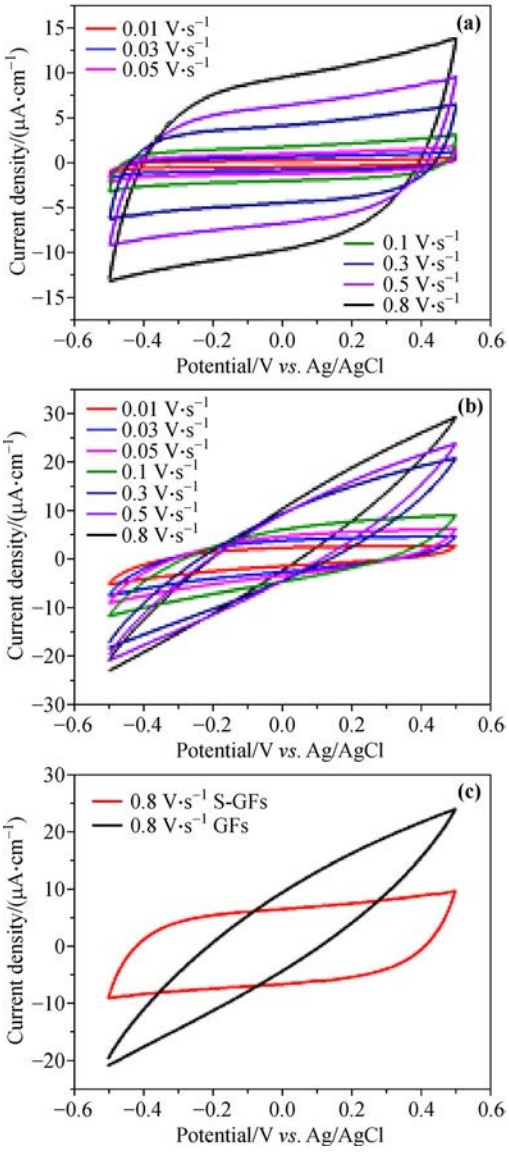

Fig. 4 CV curves: **(a)** S-GFs and **(b)** pure GFs at different scan rates; **(c)** at the scan rate of 800 $mV \cdot s^{-1}$ for S-GFs and pure GFs. All the CV curves were got in a three-electrode system with the electrolyte of 1 $mol \cdot L^{-1}$ $LiClO_4$ aqueous solution. The lengths of all samples were 1.2 cm.

double layers and effective ion transport [44]. The quasi-rectangular shape kept well even when the scan rate reached up to 2 $V \cdot s^{-1}$ (Fig. S6(a)). The energy density (E) and the power density (P) of the fiber micro-SC are shown in Fig. S7. Calculations of the specific capacitance (C), E and P of the fibriform micro-SC are demonstrated in detail in the part of Supplementary information [18,42,44].

As the mass of a fiber supercapacitor is typically low induced by its special 1D configuration, the areal capacitance or the length capacitance is more useful to compare with others [44,51]. Figure 6(b) reveals GCD

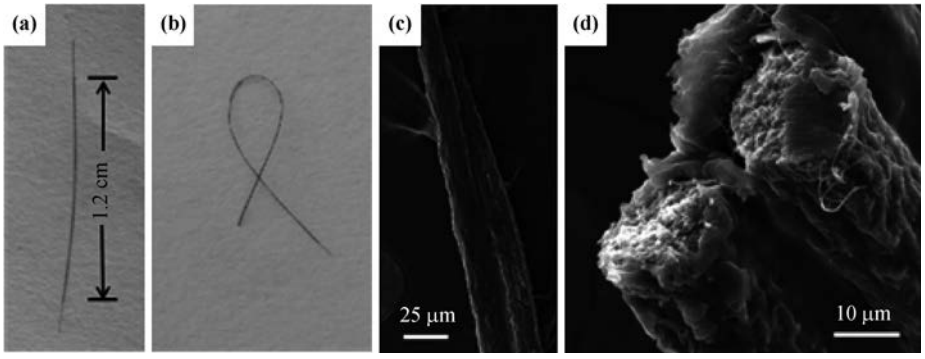

Fig. 5 Photographs of an S-GF micro-SC **(a)** in the straight status and **(b)** in the bending status with the functioning length of 1.2 cm. SEM images of **(c)** the fiber micro-SC and **(d)** its cross-section view.

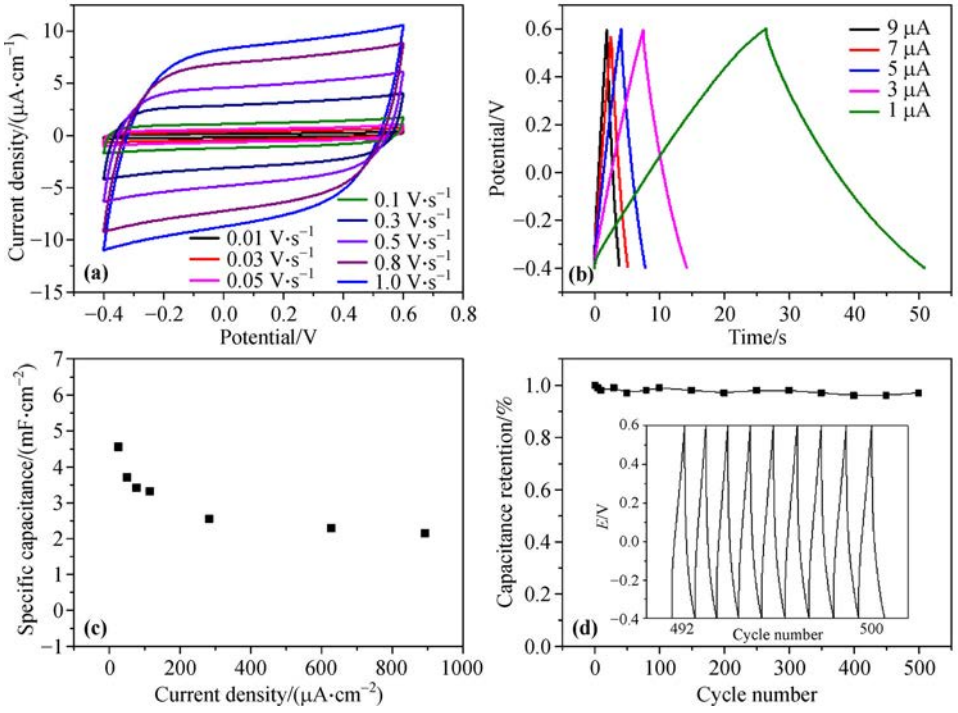

Fig. 6 Electrochemical characterization of a fiber micro-SC with the length of 1 cm in a two-electrode system: **(a)** CV curves with the scan rate ranging from 0.01 to 1 $V \cdot s^{-1}$. **(b)** GCD curves (current density: 25.47–890 $\mu A \cdot cm^{-2}$). **(c)** Areal specific capacitances corresponding to different current densities. **(d)** Cycle testing at the current density of 282 $\mu A \cdot cm^{-2}$ and the voltage of 1 V (the inset: GCD curves after 500 cycles).

curves of a fibriform capacitor with the functioning length of 1 cm, and the areal capacitance is 2.14–4.55 $mF \cdot cm^{-2}$ when the current density ranges from 25.47 to 890 $\mu A \cdot cm^{-2}$ (Figs. 5(c) and S6(b)). Moreover, the fibriform micro-SC shows high electrochemical cyclability, with 97% capacitance retained after 500 charge–discharge cycles (Fig. 6(d)).

The fibriform micro-SC has flexibility inherited from flexible S-GF electrodes. We tested the stability and the flexibility of the fibriform micro-SC using CV and GCD methods by the straight–bending–straight cycle with a bending angle of 120° (the angle was measured by the method described in Fig. S8(b)), as is seen in Fig. 7(a). The almost overlapped CV curves in Fig. 7(b) are obtained when the scan rate is 100 $mV \cdot s^{-1}$. The GCD curves with a typical triangular shape in Fig. 7(c), which are tested at a current density of 70.12 $\mu A \cdot cm^{-2}$, are almost overlapped too. Such overlapped CV and GCD curves indicate that the supercapacitor has the advantages of high flexibility and electrochemical stability. The areal capacitance is about 3.4

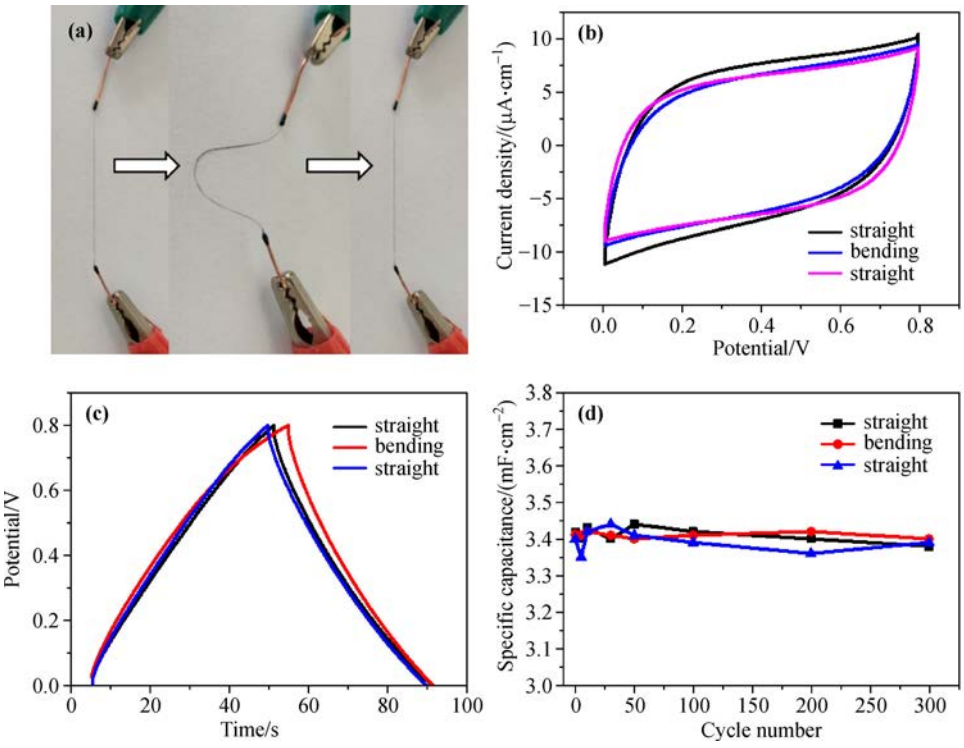

Fig. 7 **(a)** Photographs of the fiber micro-SCs with the active length of 1.2 cm during a straight–bending–straight cycle. **(b)** CV curves and **(c)** GCD curves of the fiber micro-SC during a straight–bending–straight cycle. **(d)** The stable specific capacitance during 300 straight–bending–straight cycles.

$mF \cdot cm^{-2}$ with a current density of 70.12 $\mu A \cdot cm^{-2}$ during 300 straight–bending–straight cycles, also demonstrating electrochemical stability and flexibility (Fig. 7(d)). Can the bending angle influence the capacitance of the fiber micro-SC? We have also studied this problem. Figures S8(c) and S8(d) imply that with the increase of the bending angle (0°, 120°, 150° and 170° corresponding to different statuses shown in Fig. S8(a)), the specific capacitance of the fiber micro-SC drops slightly.

4 Conclusions

In conclusion, we used the hydrothermal strategy, the *in situ* interfacial polymerization method and the annealing method to fabricate a novel type of S-GFs with better electrochemical properties than those of pure GFs when used in flexible fibriform micro-SCs. An all-solid-state fibriform micro-SC, assembled with two S-GFs, displayed flexibility and had a high areal specific capacitance of 4.55 $mF \cdot cm^{-2}$ when the current density was 25.47 $\mu A \cdot cm^{-2}$. The CV curve of the micro-SC kept a rectangular shape well even when the scan rate reached up to 2 $V \cdot s^{-1}$, and the electrochemical window could be as wide as 1 V. This type of S-GFs may help contribute to the development of flexible wearable electronics, and the methods of doping heteroatoms and assembling capacitors described in this study are also applicable to the development of graphene-based fibriform supercapacitors.

Disclosure of potential conflicts of interests The authors declare that they have no conflicts of interest.

Acknowledgements Thank for the National Natural Science Foundation of China (Grant No. 51602358) to support this work, and also thank for the High Level Personnel Fund of Zhoukou Normal University (ZKNU2014117) and the Education Department of Henan Province Natural Science Research Program (18B150029). L.J. acknowledges the Key Laboratory of Polymeric Composite & Functional Materials of Ministry of Education for funding (PCFM-2017-04).

References

[1] Sun H, You X, Deng J, et al. Novel graphene/carbon nanotube composite fibers for efficient wire-shaped miniature energy devices. Advanced Materials, 2014, 26(18): 2868–2873

[2] Lee S Y, Choi K H, Choi W S, et al. Progress in flexible energy storage and conversion systems, with a focus on cable-type lithium-ion batteries. Energy & Environmental Science, 2013, 6 (8): 2414–2423

[3] Cheng H H, Hu C G, Zhao Y, et al. Graphene fiber: a new material platform for unique applications. NPG Asia Materials, 2014, 6(7): e113

[4] Zeng W, Shu L, Li Q, et al. Fiber-based wearable electronics: a review of materials, fabrication, devices, and applications. Advanced Materials, 2014, 26(31): 5310–5336

[5] Cheng H, Liu J, Zhao Y, et al. Graphene fibers with predetermined deformation as moisture-triggered actuators and robots. Angewandte Chemie International Edition, 2013, 52(40): 10482–10486

[6] Lee E J, Choi S Y, Jeong H, et al. Active control of all-fibre graphene devices with electrical gating. Nature Communications, 2015, 6(1): 6851 (6 pages)

[7] Li Y, Sheng K, Yuan W, et al. A high-performance flexible fibre-shaped electrochemical capacitor based on electrochemically reduced graphene oxide. Chemical Communications, 2013, 49 (3): 291–293

[8] Shao C, Xu T, Gao J, et al. Flexible and integrated supercapacitor with tunable energy storage. Nanoscale, 2017, 9(34): 12324–12329

[9] Liao M, Sun H, Zhang J, et al. Multicolor, fluorescent supercapacitor fiber. Small, 2017, 14(43): 1702052 (6 pages)

[10] Dong Z, Jiang C, Cheng H, et al. Facile fabrication of light, flexible and multifunctional graphene fibers. Advanced Materials, 2012, 24(14): 1856–1861

[11] Xu Z, Gao C. Graphene chiral liquid crystals and macroscopic assembled fibres. Nature Communications, 2011, 2(1): 571–580

[12] Cong H P, Ren X C, Wang P, et al. Wet-spinning assembly of continuous, neat, and macroscopic graphene fibers. Scientific Reports, 2012, 2(1): 613–619

[13] Tian Q, Xu Z, Liu Y, et al. Dry spinning approach to continuous graphene fibers with high toughness. Nanoscale, 2017, 9(34): 12335–12342

[14] Ma T, Gao H L, Cong H P, et al. A bioinspired interface design for improving the strength and electrical conductivity of graphene-based fibers. Advanced Materials, 2018, 30(15): 1706435

[15] Xu Z, Gao C. Graphene fiber: a new trend in carbon fibers. Materials Today, 2015, 18(9): 480–492

[16] Aboutalebi S H, Jalili R, Esrafilzadeh D, et al. High-performance multifunctional graphene yarns: toward wearable all-carbon energy storage textiles. ACS Nano, 2014, 8(3): 2456–2466

[17] Bae J, Park Y J, Lee M, et al. Single-fiber-based hybridization of energy converters and storage units using graphene as electrodes. Advanced Materials, 2011, 23(30): 3446–3449

[18] Meng Y, Zhao Y, Hu C, et al. All-graphene core–sheath microfibers for all-solid-state, stretchable fibriform supercapacitors and wearable electronic textiles. Advanced Materials, 2013, 25(16): 2326–2331

[19] Zheng B N, Huang T Q, Kou L, et al. Graphene fiber-based asymmetric micro-supercapacitors. Journal of Materials Chemistry A: Materials for Energy and Sustainability, 2014, 2(25): 9736–9743

[20] Li X, Zang X, Li Z, et al. Large-area flexible core–shell graphene/porous carbon woven fabric films for fiber supercapacitor electrodes. Advanced Functional Materials, 2013, 23(38): 4862–4869

[21] Wang X, Liu B, Liu R, et al. Fiber-based flexible all-solid-state asymmetric supercapacitors for integrated photodetecting system. Angewandte Chemie International Edition, 2014, 53(7): 1849–1853

[22] Hu Y, Cheng H, Zhao F, et al. All-in-one graphene fiber supercapacitor. Nanoscale, 2014, 6(12): 6448–6451

[23] Ding X T, Zhao Y, Hu C G, et al. Spinning fabrication of graphene/polypyrrole composite fibers for all-solid-state, flexible fibriform supercapacitors. Journal of Materials Chemistry A: Materials for Energy and Sustainability, 2014, 2(31): 12355–12360

[24] Chen Q, Meng Y N, Hu C G, et al. MnO_2-modified hierarchical graphene fiber electrochemical supercapacitor. Journal of Power Sources, 2014, 247: 32–39

[25] Li Z, Xu Z, Liu Y, et al. Multifunctional non-woven fabrics of interfused graphene fibres. Nature Communications, 2016, 7(1): 13684

[26] Xu T, Ding X, Liang Y, et al. Direct spinning of fiber supercapacitor. Nanoscale, 2016, 8(24): 12113–12117

[27] Qu G, Cheng J, Li X, et al. A fiber supercapacitor with high energy density based on hollow graphene/conducting polymer fiber electrode. Advanced Materials, 2016, 28(19): 3646–3652

[28] Liang Y, Wang Z, Huang J, et al. Series of in-fiber graphene supercapacitors for flexible wearable devices. Journal of Materials Chemistry A: Materials for Energy and Sustainability, 2015, 3(6): 2547–2551

[29] Wang Z P, Cheng J L, Guan Q, et al. All-in-one fiber for stretchable fiber-shaped tandem supercapacitors. Nano Energy, 2018, 45: 210–219

[30] Ji H, Wang T, Liu Y, et al. A novel approach for sulfur-doped hierarchically porous carbon with excellent capacitance for electrochemical energy storage. Chemical Communications, 2016, 52(86): 12725–12728

[31] Han J, Zhang L L, Lee S, et al. Generation of B-doped graphene nanoplatelets using a solution process and their supercapacitor applications. ACS Nano, 2013, 7(1): 19–26

[32] Wang D W, Li F, Chen Z G, et al. Synthesis and electrochemical property of boron-doped mesoporous carbon in supercapacitor. Chemistry of Materials, 2008, 20(22): 7195–7200

[33] Guo H, Gao Q. Boron and nitrogen co-doped porous carbon and its enhanced properties as supercapacitor. Journal of Power

Sources, 2009, 186(2): 551–556

[34] Kwon T, Nishihara H, Itoi H, et al. Enhancement mechanism of electrochemical capacitance in nitrogen-/boron-doped carbons with uniform straight nanochannels. Langmuir, 2009, 25(19): 11961–11968

[35] Wu G, Tan P F, Wu X J, et al. High-performance wearable micro-supercapacitors based on microfluidic-directed nitrogen-doped graphene fiber electrodes. Advanced Functional Materials, 2017, 27(36): 1702493

[36] Peng Z, Ye R, Mann J A, et al. Flexible boron-doped laser-induced graphene microsupercapacitors. ACS Nano, 2015, 9(6): 5868–5875

[37] Yang Z, Yao Z, Li G, et al. Sulfur-doped graphene as an efficient metal-free cathode catalyst for oxygen reduction. ACS Nano, 2012, 6(1): 205–211

[38] Fan J J, Fan Y J, Wang R X, et al. A novel strategy for the synthesis of sulfur-doped carbon nanotubes as a highly efficient Pt catalyst support toward the methanol oxidation reaction. Journal of Materials Chemistry A: Materials for Energy and Sustainability, 2017, 5(36): 19467–19475

[39] Yang S B, Zhi L J, Tang K, et al. Efficient synthesis of heteroatom (N or S)-doped graphene based on ultrathin graphene oxide-porous silica sheets for oxygen reduction reactions. Advanced Functional Materials, 2012, 22(17): 3634–3640

[40] Yang Z, Yao Z, Li G, et al. Sulfur-doped graphene as an efficient metal-free cathode catalyst for oxygen reduction. ACS Nano, 2012, 6(1): 205–211

[41] Wu Z S, Parvez K, Winter A, et al. Layer-by-layer assembled heteroatom-doped graphene films with ultrahigh volumetric capacitance and rate capability for micro-supercapacitors. Advanced Materials, 2014, 26(26): 4552–4558

[42] Wang Y. Research progress on anovel conductive polymer–poly (3,4-ethylenedioxythiophene) (PEDOT). Journal of Physics: Conference Series, 2009, 152: 012023

[43] Jin L, Wang T, Feng Z Q, et al. A facile approach for the fabrication of core–shell PEDOT nanofiber mats with superior mechanical properties and niocompatibility. Journal of Materials Chemistry B: Materials for Biology and Medicine, 2013, 1(13): 1818–1825

[44] Meng Y N, Jin L, Cai B, et al. Facile fabrication of flexible core–shell graphene/conducting polymer microfibers for fibriform supercapacitors. RSC Advances, 2017, 7(61): 38187–38192

[45] Cai S Y, Huang T Q, Chen H, et al. Wet-spinning of ternary synergistic coaxial fibers for high performance yarn super-capacitors. Journal of Materials Chemistry A: Materials for Energy and Sustainability, 2017, 5(43): 22489–22494

[46] Liu H, Liu Y, Zhu D. Chemical doping of graphene. Journal of Materials Chemistry, 2011, 21(10): 3335–3345

[47] Sheng Z H, Shao L, Chen J J, et al. Catalyst-free synthesis of nitrogen-doped graphene via thermal annealing graphite oxide with melamine and its excellent electrocatalysis. ACS Nano, 2011, 5(6): 4350–4358

[48] Li X, Wang H, Robinson J T, et al. Simultaneous nitrogen doping and reduction of graphene oxide. Journal of the American Chemical Society, 2009, 131(43): 15939–15944

[49] Cui Z, Li C M, Jiang S P. PtRu catalysts supported on heteropolyacid and chitosan functionalized carbon nanotubes for methanol oxidation reaction of fuel cells. Physical Chemistry Chemical Physics, 2011, 13(36): 16349–16357

[50] Hu D, He X, Sun L, et al. Growth of single-salled carbon nanotubes from Ag_{15} cluster catalysts. Science Bulletin, 2016, 61 (12): 917–920

[51] Yu D, Qian Q, Wei L, et al. Emergence of fiber supercapacitors. Chemical Society Reviews, 2015, 44(3): 647–662

Supplementary information

Calculations of electrochemical parameters of the fibriform sulfur-doped micro-SC

The specific capacitance (C), the energy density (E) and the power density (P) of the fibriform sulfur-doped micro-SC are calculated on the basis of GCD curves. Specific measures are as follows (Eqs. (S1) and (S2)):

$$C = I/(\mathrm{d}U/\mathrm{d}t) \tag{S1}$$

where I and $\mathrm{d}U/\mathrm{d}t$ are the discharge current and the slope of the discharge curve, respectively.

The areal capacitance (C_A) can be calculated by Eq. (S2):

$$C_\mathrm{A} = C/A \tag{S2}$$

where A is the surface area of the fiber electrode and is based on Eq. (S3):

$$A = \pi DL \tag{S3}$$

where D is the diameter of the fiber electrode and L is the active length of the device.

E and P of the fibriform micro-SC are obtained from Eqs. (S4) and (S5):

$$E = 0.5 C_\mathrm{A} U^2/3600 \tag{S4}$$

$$P = 3600E/t_\mathrm{discharge} \tag{S5}$$

where U and $t_\mathrm{discharge}$ represent the operating voltage and the discharge time, respectively. In Eqs. (S4) and (S5), the units of E, C_A, U, P and $t_\mathrm{discharge}$ are $\mathrm{W\cdot h\cdot cm^{-2}}$, $\mathrm{F\cdot cm^{-2}}$, V, $\mathrm{W\cdot cm^{-2}}$ and s, respectively.